Microstructural and Mechanical Characterization of Catalyst Coated Membranes Subjected to In Situ Hygrothermal Fatigue

Alireza Sadeghi Alavijeh,[a] Ramin M.H. Khorasany,[a] Zachary Nunn,[a] Aronne Habisch,[a] Michael Lauritzen,[b,*] Erin Rogers,[b] G. Gary Wang,[a] and Erik Kjeang[a,*,z]

[a]*School of Mechatronic Systems Engineering, Simon Fraser University, Surrey, British Columbia V3T 0A3, Canada*
[b]*Ballard Power Systems, Burnaby, British Columbia V5J 5J8, Canada*

Catalyst coated membranes (CCMs) in polymer electrolyte fuel cells are subjected to mechanical stresses in the form of fatigue and creep that deteriorate the durability and lifetime of the cells. The present article aims to determine the effect of in-situ hygrothermal fatigue on the microstructure and mechanical properties of the CCM. The fatigue process is systematically explored by the application of two custom-developed accelerated mechanical stress test (AMST) experiments with periodic extraction of partially degraded CCMs. Cross sectional and top surface scanning electron microscope (SEM) images of the end-of-test CCMs reveal the formation of mechanically induced cracks and delamination due to cyclic tensile and compressive fatigue stress. Tensile and expansion tests are conducted at different stages of degradation to evaluate the evolution in the mechanical and hygrothermal properties of the CCM. The tensile test results indicate gradual reductions in final strain, ultimate tensile strength, and fracture toughness with increasing number of fatigue cycles. The decay in tensile properties is attributed to the microstructural damage and micro-cracks formed during the AMST. Moreover, it is shown that the hygrothermal expansion of the CCM is more sensitive to conditioning than mechanical degradation.

Manuscript submitted June 5, 2015; revised manuscript received September 28, 2015. Published October 10, 2015.

Polymer electrolyte fuel cells (PEFCs) are a prime candidate to replace gasoline and diesel internal combustion engines for transportation applications due to their environmental benefits combined with rapid start-up, high efficiency, and high power density at relatively low operating temperature.[1] The commercialization of PEFCs is dependent on the development of membrane electrode assemblies (MEA) capable of meeting the automotive industry durability targets.[2] However, the current PEFC technology is facing insufficient longevity, mainly because of the deterioration of the proton exchange membrane (PEM) component.[1] Hence, an essential step to accomplish the commercialization requirements for PEFCs is to enhance the membrane durability and lifetime. Among various types of membranes utilized in PEFCs, perfluorosulfonic acid (PFSA) ionomer membranes (e.g., Nafion from DuPont) are the most widely used materials due to the superior chemical stability attributed to the chemically inert C-F bonds of the polytetrafluoroethylene (PTFE) base structure.[3]

Chemical and mechanical degradation mechanisms are recognized as the principal root causes for lifetime limiting failures of PFSA ionomer membranes in fuel cells. Understanding of the degradation mechanisms, their interactions, and the corresponding failure modes could provide valuable insight toward decelerating the rate of the membrane degradation and thereby extend the lifetime.[2] Chemical degradation is caused by the attack of radical species in the form of hydroxyl (•OH) and hydroperoxyl (•OOH) radicals generated through decomposition of hydrogen peroxide (H_2O_2) by metal contaminants.[2,4,5] Hydroxyl radicals also form as a by-product of the electrochemical reaction between H_2 and O_2 on the surface of Pt due to gas crossover.[6] Mechanical degradation, on the other hand, is originated by the hygrothermal stresses induced by fluctuations in the relative humidity and temperature. Membrane swelling and contraction due to water sorption coupled with the constrained geometry of the membrane in between the catalyst layers, gas diffusion layers, and bipolar plates in the PEFC introduce mechanical stresses inside the membrane.[7] During fuel cell operation, poor humidification and dry conditions result in the shrinkage and in-plane tension, while wet conditions lead to swelling and in-plane compression in the membrane.[2]

Mechanical strength and endurance of the thin PFSA membrane layer are critical for the membrane to remain intact against the in-situ hygrothermal cyclic stresses. Current efforts in reducing the ohmic losses and enhancing the PEFC performance can be facilitated through developing thinner but mechanically stable ionomer membranes. Hence, mechanical properties of PFSA membranes individually[8–12] or in composite with the catalyst layers[13–16] were thoroughly investigated. Kundu et al.[8] studied the tensile properties of PFSA membranes under dry and fully hydrated conditions and showed the sensitivity of the membrane elastic modulus and yield strength to the changes in relative humidity. Similar dependency between the membrane mechanical behavior and environmental conditions was reported by Tang et al.[9] and Bauer et al.[10] on Nafion 112 and 117, respectively. Tang et al.[11] attained the fatigue strength of Nafion 111 around 10% of the tensile strength via performing cyclic fatigue loading. In addition, mechanical degradation of Nafion NR-211 membrane was investigated by our group[12] through conducting ex-situ uniaxial fatigue-fracture experiments under a range of temperature and humidity conditions. According to the results of this study, the fatigue endurance is substantially reduced by worsening the environmental conditions, in particular for elevated temperatures such as those used during automotive fuel cell operation.

Additional research on catalyst coated membrane (CCM) composite materials having a common, linked ionomer phase indicated notable differences between the mechanical properties of pure PFSA membranes and CCMs. Mechanical properties of CCM composites were comprehensively investigated by our group and compared to those of the corresponding PFSA membranes.[14–17] By conducting tensile stress-strain and dehydration tests under a wide range of temperature and RH conditions, Goulet et al.[14] evaluated the intrinsic mechanical properties of the CCM and compared them to the PFSA membrane. The time dependent mechanical response of the CCM to variations in temperature, RH, and tensile stress was recently assessed by Sadeghi et al.[16] through tensile creep and recovery tests. Both studies revealed significant reinforcement obtained when the membrane is coated with catalyst layers.[14,16] Furthermore, the CCM tensile and dynamic mechanical properties were found to be more sensitive to temperature than RH.[14,16] The confinement imposed to the membrane by the catalyst and diffusion layers was shown to prevent in-plane expansion/contraction, hence resulting in lower tensile peak stress when compared to the pure

*Electrochemical Society Active Member.
[z]E-mail: ekjeang@sfu.ca

membrane, while the through-plane stress and strain were increased during hydration.[17]

In order to evaluate the durability and diagnose potential mitigation strategies at reasonable cost and time, accelerated stress testing (AST) is generally applied via aggravating the chemical and mechanical stressors including current density, cell voltage, temperature, and RH fluctuations.[2,4,18] Open circuit voltage (OCV)[13,18–23] and RH cycling[24–30] AST protocols are generally utilized to exacerbate the rate of chemical and mechanical degradation, respectively. Lai et al.[24] performed in-situ humidity cycling tests on different membranes exposed to various RH swings and reported that the time-to-failure was extended as the membranes were subjected to smaller humidity swings. As a result of 1,200 RH cycles, Kang and Kim[25] observed delamination of membrane, catalyst layers, and gas diffusion layers as well as internal deterioration of the catalyst layers. Banan et al.[26] investigated the effects of hygrothermal cycles and external vibrations on the damage propagation and lifetime using a two-dimensional model. Although both mechanisms contributed to degradation, hygrothermal swings dominated the crack propagation while vibrations mainly governed the delamination.[26] Aindow and O'Neill[28] proposed an ex-situ approach to characterize the mechanical stability and predict the remaining lifetime of the membrane under RH cycling conditions. The rate of degradation during RH cycling was characterized by Vengatesan et al.,[29] indicating gradual decay in fuel cell performance in the initial stage followed by rapid performance loss after certain levels of degradation. Khattra et al.[30] modeled the time-dependent in-plane stresses induced inside the PFSA membrane under hydration and dehydration following two RH cycling protocols. Furthermore, in order to achieve the hydration gradient during real fuel cell operating conditions, Khattra et al.[30] also applied saturated air to the cathode while subjecting the anode side to RH cycling, and observed lower stresses inside the membrane when compared to uniform RH loading at both sides. In our group, Lim et al.[31] investigated the combined chemical and mechanical membrane degradation by following Ballard Power Systems' cyclic open circuit voltage (COCV) AST protocol and revealed that the mutual contributions of the degradation stressors exacerbated the rate of degradation and led to earlier failure.[31] The same protocol was subsequently applied to evaluate the durability enhancement obtained by coating cerium oxide (CeO_2) on the anode and cathode,[32] indicating remarkable increase in time to failure, 40x reduction in fluoride emission, and retained mechanical toughness and ductility. Additionally, Macauley et al.[33] developed and utilized an accelerated membrane durability test (AMDT) to characterize membrane stability under isolated chemical, mainly mechanical, and combined chemical and mechanical degradation using conditions relevant for field operation. The AMDT lifetime was extended in the absence of mechanical degradation by removing the RH swings and in the presence of a platinum band in the membrane.[33] According to the obtained results, formation of the platinum band thoroughly reduced the rate of chemical degradation and thereby mitigated the decay in mechanical properties and enhanced the overall durability of the membrane.[33–36] However, negative effects have also been reported[37–42] due to direct formation of radicals in a Fenton's reagent mechanism.[38–42]

In the context of membrane mechanical properties, Huang et al.[13] evaluated and compared MEAs subjected to isolated chemical degradation at OCV and isolated mechanical creep degradation during humidity cycling. Fracture strains obtained by tensile testing showed rapid reduction in the OCV degraded MEAs while it was less dramatic, though still significant, in the creep degraded MEAs.[13] The humidity cycles were conducted using relatively long humidity steps of 30 min duration with small amplitudes from 30% to 80% and from 80% to 120% RH,[13] hence mainly introducing creep stresses to the membrane analogous to the creep-recovery cycles reported in.[16] The decay in mechanical properties of CCMs subjected to combined chemical and mechanical degradation was systematically examined by our group[43] using tensile and expansion experiments in order to capture both time-independent and time-dependent mechanical responses of the CCM. In this case, the supplementary expansion experiments were found to provide a novel, insightful bridge between the in-situ swelling and contraction due to hygrothermal swings and the ex-situ measured tensile properties.

The objective of the present work is to comprehensively investigate the microstructural and mechanical properties of in-situ fatigue degraded catalyst coated membranes. Contrary to the previous study on creep-recovery under mild humidity steps,[13] the present work is focused on a custom-developed, aggressive fatigue based mechanical AST procedure that applies rapid cycling between fully wet and fully dry membrane states. In addition, the effect of accelerated mechanical stress testing (AMST) factors including wet/dry cycle frequency and operating temperature are thoroughly evaluated. Another novel element of the proposed in-situ AMST is to completely eliminate influences from chemical exposure and degradation by exclusive use of inert gas and by avoiding electrochemical diagnostics during the experiments. The obtained tensile and time-dependent hygrothermal properties are compared with the previously reported mechanical properties of CCMs subjected to combined chemical and mechanical degradation[43] in order to elucidate the role of pure mechanical fatigue stress on the in-situ degradation of PFSA membranes in PEFCs.

Experimental

In-situ fatigue testing.— The membrane electrode assemblies (MEAs) used in this work were fabricated using a previously reported procedure[43] by coating catalyst layers containing carbon supported platinum and perfluorosulfonic acid (PFSA) ionomer on micro-porous layers covered gas diffusion layer (GDL) substrates to form gas diffusion electrodes (GDEs). Anode and cathode GDEs were hot pressed with a Nafion NR-211 non-reinforced PFSA ionomer membrane to obtain an MEA. Research-scale stacks consisting of five cells with 45 cm^2 active area were assembled in a standard test hardware. Minimum pressure drop and near-uniform conditions were ensured from inlet to outlet utilizing co-flow parallel straight channels. Prior to testing, the stack was conditioned for 20 hours in humidified nitrogen gas at 100% RH to ensure fully humidified cells.

In-situ fatigue degradation was induced using a custom-developed accelerated mechanical stress test (AMST) procedure based in part on the US Department of Energy accelerated stress test (AST) for mechanical membrane degradation. The AMST is designed to generate membrane fatigue by application of rapid, deep wet/dry cycles at relatively high temperature and ambient pressure. Two distinct AMST experiments were devised under slightly different testing conditions, as detailed in Table I and further illustrated in Figure 1. The first experiment (AMST-1) applied successive cycles of 2 min wet (90% RH) and 2 min dry (0% RH) states at 80°C (Figure 1a), while the second experiment (AMST-2) was carried out using 1 min wet (100% RH) and 3 min dry (0% RH) states at 95°C (Figure 1b). The latter experiment was subjected to harsher fatigue conditions due to higher temperature and larger wet/dry (stress) amplitude. The original AST protocol[44] utilized air as the fuel/oxidant gas while in the present AMST, air was replaced by nitrogen in order to diminish any occurrence of chemical degradation. Besides applying nitrogen as the fuel/oxidant gas, electrochemical diagnostics such as in-situ leak tests, polarization and impedance measurements were avoided in order to ensure complete elimination of chemical stress and exposure throughout the AMST operation. During the wet phase, water was injected into the humidifier to preserve oversaturated inlet gas while a relatively dry state was obtained by simply terminating the flow of water. Lower gas flow rates were applied in AMST-2 due to the available constraints on the test station at elevated temperature. The stack temperature and outlet gas temperature were controlled according to the target values specified in Table I, while the inlet gas temperature was monitored to ensure that no excessively heated gas was fed into the stack. The inlet gas temperature was somewhat higher in the wet phase compared to the dry phase due to the concurrently high temperature and humidity. The wet/dry fatigue cycling was pursued until failure (crossover > 10 sccm per cell) or 20,000 cycles,[44] whichever occurred first, while one cell being extracted and replaced by a new cell every 4,000 cycles in order

Table I. Custom-developed accelerated mechanical stress test (AMST) procedures utilized in this work in order to generate in-situ membrane fatigue.

	Test I	Test II
Duration	Crossover (>10 sccm) or 20,000 cycles	Crossover (>10 sccm) or 20,000 cycles
Temperature	80°C	95°C
Wet/dry cycles	2 min dry state (~0% RH) + 2 min wet state (~90% RH)	3 min dry state (~0% RH) + 1 min wet state (~100% RH)
Fuel/Oxidant	N_2/N_2 on both sides	N_2/N_2 on both sides
Pressure	Ambient	Ambient
Flow rate	9.0 slpm	3.5 slpm

to obtain partially degraded MEAs for ex-situ characterization. The presence of through plane leaks across the membrane was evaluated qualitatively by performing a bubble jig test on the entire stack every 4,000 cycles by submerging each individual cell in water while air at 2 psig and atmospheric pressure was applied to each side of the cell. The corresponding crossover rate was calculated from the volume of air displaced at a certain time.

Ex-situ characterization.— Upon completion of the in-situ fatigue experiments, the microstructural and mechanical properties of the partially degraded MEAs were evaluated ex-situ. The locations of membrane leaks were determined on the end-of-test (fully degraded) MEAs using an FLIR T620 IR camera. At the IR benchmarked locations, surface analysis microscopy was conducted with a JEOL JSM-6360 scanning electron microscope (SEM) with integrated energy dispersive spectroscopy (EDS) analyzer. CCM samples for SEM surface analysis were cut from the MEA and the GDLs were removed from the sides of the samples. In addition to the surface analysis, SEM cross sectional backscattered electron (BSE) imaging at 20 kV was performed at the inlet, middle, and outlet positions of the end-of-test MEAs to evaluate the type and distribution of mechanical damage formed during the wet/dry cycles and to measure the level of the membrane thinning during the AMST. Cross sectional SEM samples were obtained by casting MEAs in epoxy pucks, followed by polishing with 120–1200 grit silicon carbide paper using a Struers TegraPol-11 polisher and carbon coating using an Edwards Scancoat Six Sputter Coater. The membrane thickness of the end-of-test MEAs was also measured using cross sectional SEM by taking the average of five measurements at different locations of each MEA. Finally, the platinum concentration in the membrane was measured by EDS elemental analysis.

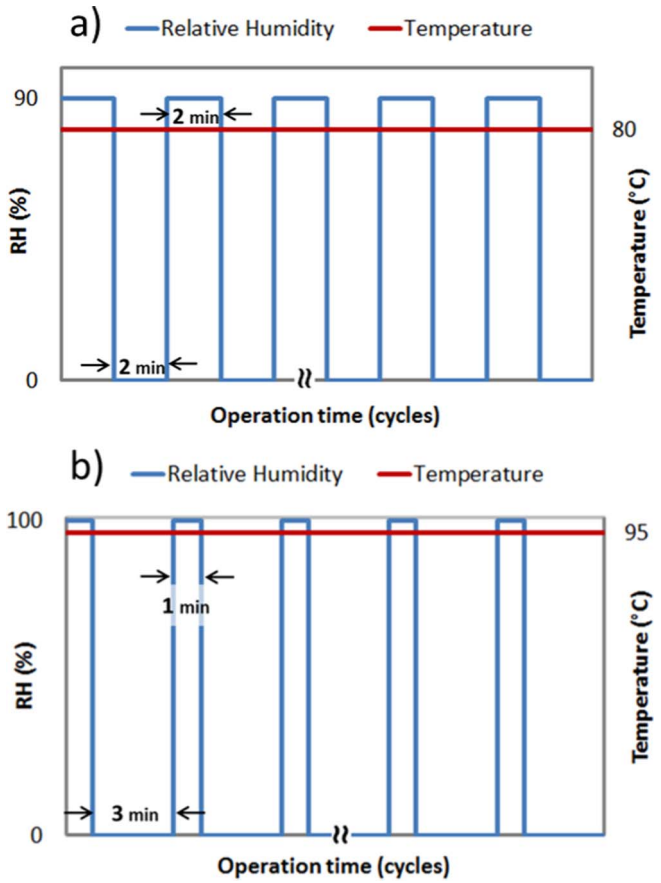

Figure 1. Schematic of the wet/dry fatigue cycles applied in the (a) AMST-1 and (b) AMST-2 experiments.

In order to investigate the decay in mechanical properties, beginning of life (BOL) and partially degraded MEAs (extracted after 4,000, 8,000, 12,000, 16,000, and 20,000 wet/dry cycles) were cut to rectangular shape (20 × 1.2 mm) along the transverse direction using a plotter cutter. The GDLs were removed from the sides of the MEAs to obtain the CCM tensile and expansion specimens. Tensile and expansion tests were performed using a dynamic mechanical analyzer (TA Instruments Q800 DMA) equipped with an environmental chamber (TA Instruments DMA-RH Accessory). The gauge length of the tensile and expansion specimens was measured by the DMA prior to each test. The average membrane thickness was calculated by subtracting the cathode and anode thicknesses from the average CCM thickness measured by a micrometer.

Tensile CCM specimens taken from the inlet section of the cells were loaded following a standardized 5:1 length to width aspect ratio to eliminate edge stress concentration.[14] The remaining length of the specimen (14 mm) was gripped and fixed under the tensile clamps. Tensile tests were conducted at fuel cell operating conditions (70°C and 90% RH) on the BOL and AMST degraded CCMs after equilibration under a small preload tensile force (0.003 N) to keep the specimens under tension. Once equilibrated, the specimens were stretched under a fixed strain rate (0.01 min^{-1}) to the fracture point or to the maximum DMA clamp travel length of about 26 mm (330% elongation for 6 mm initial length). In case of fracture near the clamp region, the obtained results were rejected and the test was repeated with another sample. The average of four tensile experiments on identical specimens was reported at each level of degradation in order to ensure consistency and statistical relevance. The variability of the measurements was also presented in the form of error bars indicating two standard deviations, which statistically covers about 95% of the data points.

Thermal and hygral expansion experiments were performed on CCMs extracted from the middle section of the cells using the same specimen dimensions, DMA instrument, gauge length, and preload force as for the previously reported tensile tests. Thermal expansion tests were conducted by measuring the axial changes in the specimen length after equilibration at fixed 90% RH while the temperature was elevated from 20°C to 40°C, 40°C to 60°C, and 60°C to 80°C. It should be noted that the membrane water content increases with temperature; therefore, the thermal expansion experiments encompass an intrinsic hygral expansion term as well. At each step, once the temperature reached the desired value, the conditions were kept constant for one hour in order to obtain the time-dependent thermal elongations. Hygral expansion tests were conducted in the same manner at fixed temperature (70°C) while the relative humidity was elevated from

0% to 30%, 30% to 50%, 50% to 70%, and 70% to 90%. Similar to the thermal expansion, the time-dependent hygral elongations were captured by keeping the desired conditions constant for one hour.

Results and Discussion

The custom-designed accelerated mechanical stress tests (AMSTs) were applied on the research scale fuel cell stacks in order to investigate the in-situ hygrothermal membrane fatigue process and generate partially degraded catalyst coated membranes (CCMs) for subsequent ex-situ characterization of the microstructural and mechanical properties. The obtained damage and leak distribution of the end-of-test CCMs were determined with IR imaging while the cross sectional and top surface microstructure was analyzed using SEM. Furthermore, CCM tensile and expansion properties were measured at different levels of fatigue degradation from BOL to 20,000 fatigue cycles. From the obtained results, tensile stress-strain curves, elastic modulus, ultimate tensile strength, final strain, and hygrothermal expansion properties are derived and discussed.

Accelerated mechanical stress tests - comparison.— Two distinct AMSTs were examined in this work, as previously summarized in Table I and Figure 1. The first experiment (AMST-1) was terminated at 20,000 cycles, after which an MEA leak rate measurement of 14 sccm per cell was obtained, indicative of membrane failure. IR imaging of the AMST-1 end-of-test MEA further revealed membrane transfer leaks at the inlet region, as shown in Figure 2a. The inlet region of the cells was exposed to slightly higher gas temperatures compared to the middle and outlet regions, which resulted in more severe degradation at the inlet. This area of the MEA was therefore preserved for subsequent top surface SEM analysis. The analysis of the ohmic resistance of the cells indicated that although the inlet gas RH was 0% during the dry phase, the membranes did not reach a stable, fully dry condition within the 2 min hold time. The ohmic resistance of the stack was therefore scaled by exposing the cells to various fixed RH levels for one hour duration, thus equilibrating the ionomer water content and conductivity at each state, with results provided in Table II. The measured ohmic resistances at the end of the wet and dry phases of AMST-1 were 0.00038 and 0.053 ohm $\cdot$ cm^{-2}, indicating that the ionomer specific temporal RH conditions had reached 90% and slightly less than 10%, respectively. It was also observed that the 90% RH condition (0.00038 ohm $\cdot$ cm^{-2}) was obtained in less than one minute of the wet phase, suggesting that the 2 min wet phase may be excessively long in duration. However, the desired fully dry state was not achieved within the 2 min dry phase. While the wet condition results in compressive stress, the dry condition at low RH results in high tensile stress in the membranes due to the constrained contraction inside the cells.[45] Therefore, in order to maximize the amplitude of the fatigue stress in each wet/dry cycle, the dry phase was prolonged in the second experiment (AMST-2) while the total duration of each wet/dry cycle was kept identical to AMST-1, i.e., using 3 min dry and 1 min wet phases. The inlet RH of the wet phase was also raised from 90% (AMST-1) to 100% (AMST-2) in order to further increase the fatigue stress amplitude, while the overall intensity of the experiment was increased by raising the test temperature from 80°C to 95°C. As a result, the ohmic resistances at the end of the wet and dry phases of AMST-2 reached 0.00033 and 0.091 ohm $\cdot$ cm^{-2}, respectively, indicating that the peak levels of both hydration and dehydration had been successfully enhanced compared to AMST-1. The periodic leak rate tests on the AMST-2 stack indicated a membrane crossover rate of ~7 sccm after 20,000 cycles, which is close to the failure criterion (>10 sccm per cell). Furthermore, the IR image of the end-of-test degraded MEA (Figure 2b) revealed the presence of leaks at the inlet region with a similar distribution compared to the previous observations for AMST-1. However, the higher brightness level observed at the inlet of the AMST-1 image compared to the surroundings suggests that the local leak was more significant than for AMST-2, which is qualitatively in agreement with the larger crossover measured by the bubble jig test of AMST-1. It should be noted that the color of each IR image was auto-adjusted according to the temperature distribution. Therefore, the relatively monotonic colors of the AMST-2 IR image (Figure 2b) indicates a marginally higher temperature at the hot spot compared to the surroundings, while the remarkably disparate colors of the hot spot and surroundings in the AMST-1 image (Figure 2a) resembles a more significant leak site.

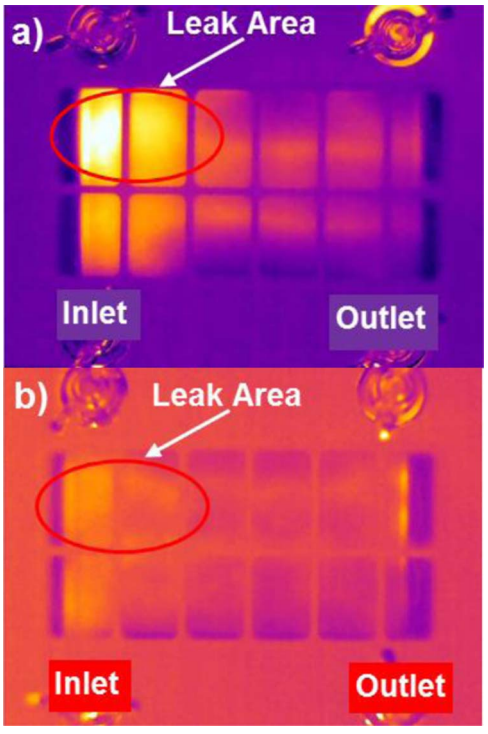

Figure 2. IR images of AMST degraded MEAs after 20,000 cycles (end-of-test) in (a) AMST-1 and (b) AMST-2. The brightness is proportional to the local temperature; hence, bright regions indicate leak locations.

Table II. Ohmic resistance of the stack upon equilibration at fixed relative humidity levels.

Relative Humidity (%)	Ohmic Resistance (ohm.cm^{-2})
0	3.1111
10	0.01111
20	0.00444
40	0.00118
60	0.00064
80	0.00044
90	0.00038
100	0.00033
120	0.00024

Microstructural analysis.— The cross sectional and top surface microstructure of the end-of-test degraded CCMs (20,000 cycles) was analyzed using SEM. Cross sectional SEM was also utilized to track the membrane thickness during the tests. Figure 3 represents the average thickness of the AMST degraded membranes at the end-of-test normalized by the original membrane thickness at BOL. The results are also compared to the end-of-life membrane thickness after combined chemical and mechanical degradation via the cyclic open circuit voltage (COCV) AST previously reported by Lim et al.[31] According to Figure 3, the average membrane thinning observed in the two AMSTs was ~4–5% and ~9%, respectively, while 48% thinning was measured for the COCV AST, notably due to severe chemical degradation which was completely eliminated in the present AMSTs. The small degree of membrane thinning detected in the AMSTs may have been

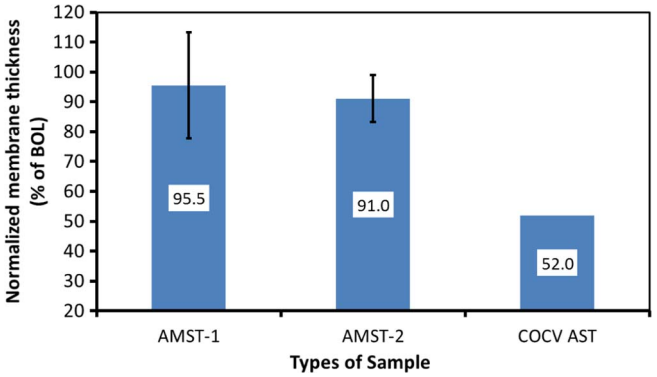

Figure 3. Normalized membrane thickness of the AMST degraded MEAs extracted after 20,000 cycles (end-of-test) compared to the end-of-life COCV AST membrane thickness reported by Lim et al.[31]

induced by in-plane visco-plastic deformation and residual stresses considering the dominant fatigue stress in this direction.[46] In addition, the more significant thickness reduction observed for AMST-2 compared to AMST-1 could be correlated to the higher stress amplitude and temperature of the second experiment.

Cross sectional SEM images resembled the initiation and propagation of mechanical damage including cracks and delamination in the membranes and catalyst layers of the AMST degraded MEAs at the end-of-test, as depicted and compared with a BOL MEA image in Figure 4. The overall membrane damage was dominated by cracks. Major cracks generally extended from the membrane into the adjacent catalyst layers, indicating significant interaction between these two components, although the exact initiation sites cannot be verified by these images. Membrane leaks and failures were likely attributed to occasional, large cracks spanning the entire membrane thickness, such as the main crack identified in Figure 4d. Careful analysis of Figures 4c and 4d also revealed the formation of small micro-cracks inside the membrane, which is likely a result of material fatigue. Local delamination of membrane and catalyst layers, as observed here, is attributed to the fatigue stress combined with the differences in hygral expansion and contraction of the membrane and catalyst layers. Due to the loss of CCM integrity in these regions, it is likely that the local membrane stresses are exacerbated in the absence of the reinforcing effect otherwise known to occur.[14,16] Qualitatively, larger and more frequent microstructural damage features were detected in the cross section of AMST-2 when compared to AMST-1, indicating that the AMST-2 MEAs were subjected to harsher conditions for mechanical membrane degradation.

Due to catalyst layer degradation under dynamic duty cycles, a Pt band is normally formed inside the membrane, which has been shown to enhance the membrane stability and lifetime.[33,34] The presence of Pt inside the AMST degraded membranes was evaluated and compared to the ones degraded by the COCV AST. The results showed no distinct formation of Pt particles in either of the AMST-1 or AMST-2 end-of-test membranes (~0 ppm) while an average of ~8,000 ppm Pt was detected in the end of life (EOL) COCV AST membrane,[31] confirming that the Pt band is originated through chemical routes which were intentionally blocked in the present AMST experiments.

Complementary top surface microstructural analysis was performed on the severely damaged regions initially identified by IR imaging, located at the inlet of the end-of-test degraded MEAs. The SEM images in Figure 5 exhibit the BOL CCM surface as a reference and typical microstructural imperfections captured on the degraded CCM surface, including cracks and detachments of the catalyst layers as well as major cracks in the membrane. As represented in Figure 5,

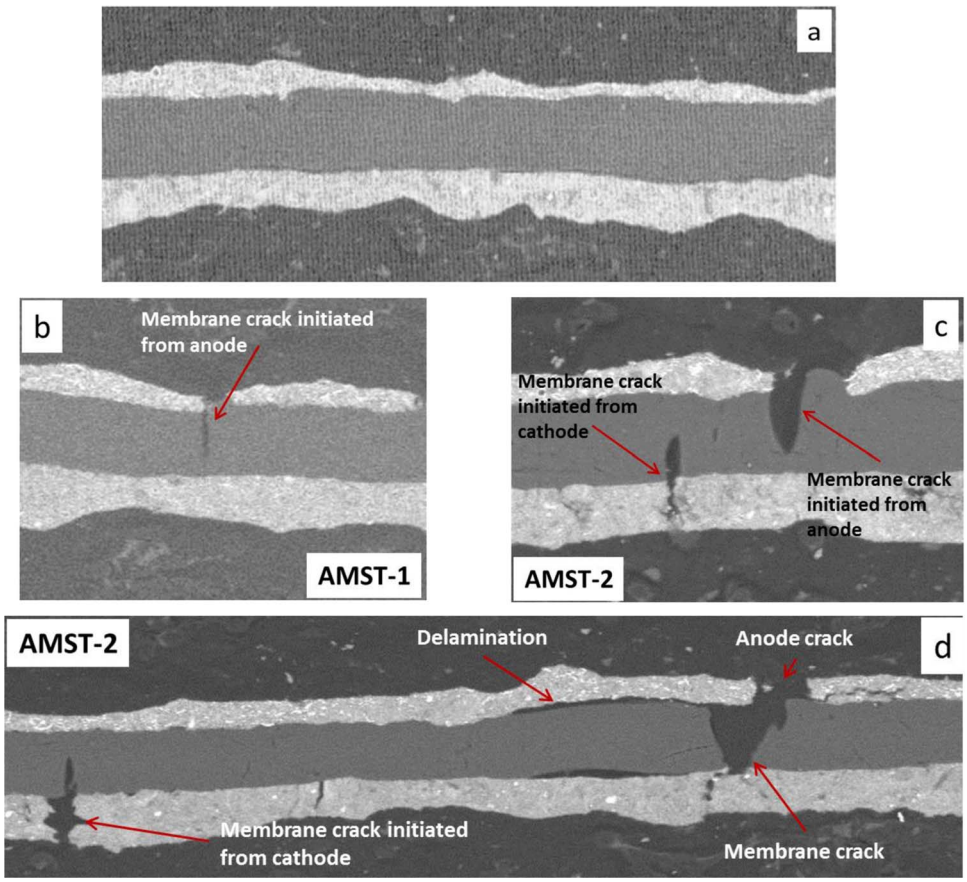

Figure 4. Cross sectional SEM images of (a) a BOL MEA and (b-d) end-of-test degraded MEAs from the (b) AMST-1 and (c, d) AMST-2 experiments.

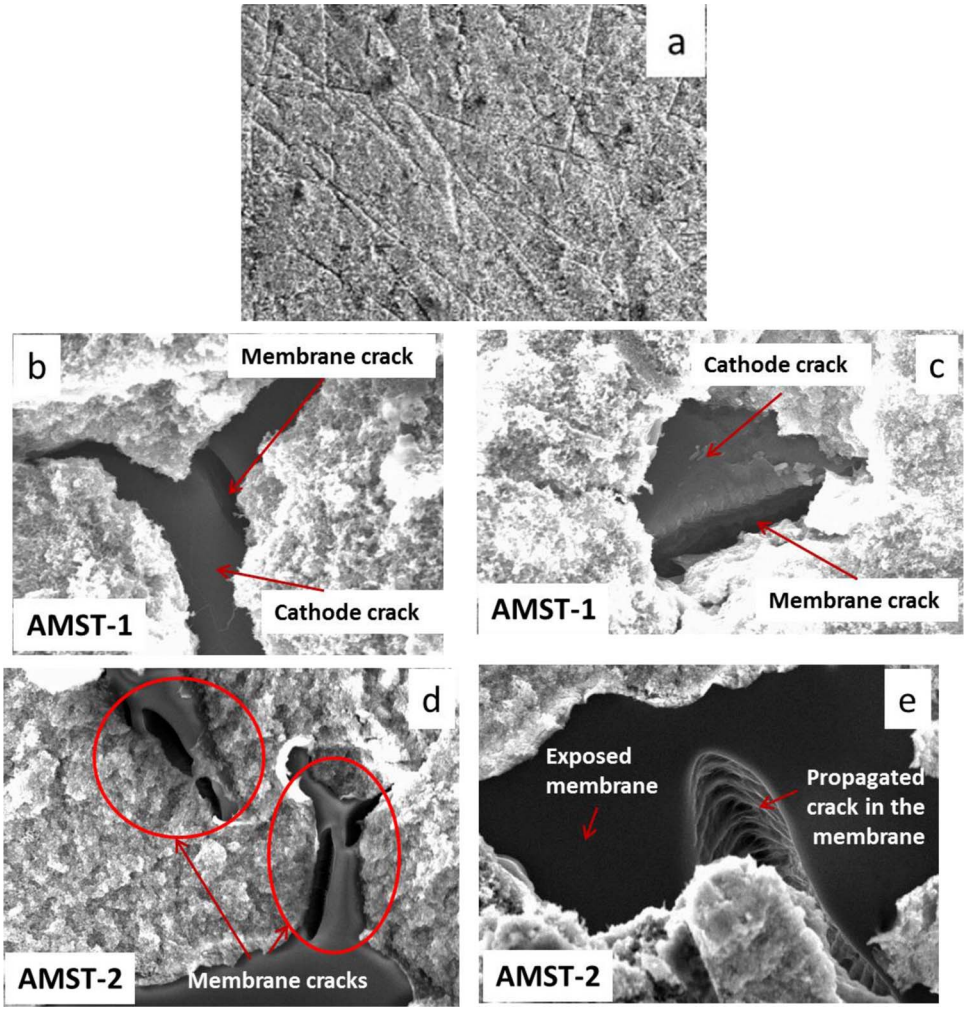

Figure 5. Top surface SEM images of (a) a BOL CCM and (b–e) end-of-test degraded CCMs from the (b,c) AMST-1 and (d,e) AMST-2 experiments. The samples were taken from the heavily damaged inlet areas detected by IR imaging (cf., Fig. 3).

cathode cracks and detachments are coupled with the cracks extended inside the membrane. This confirms the interaction between damage in the catalyst layers and membranes induced by the hygrothermal fatigue stress in the membrane. Cracks that span the entire membrane thickness are observed to extend substantially in the in-plane direction in the membrane. Similar to the cross sectional findings, more severe damage was observed in AMST-2 compared to AMST-1 due to the higher fatigue amplitude and temperature. High operating temperature leads to lower mechanical strength of the membrane and thereby increases the impact of the fatigue cycles. Additionally, a longer dry phase induces larger membrane contraction and more aggressive tensile stresses in the membrane.

Tensile properties.— Tensile tests were conducted at 70°C and 90% RH on BOL and AMST degraded CCM samples at different stages of degradation. A graphical summary of the selected stress-strain curves is presented in Figure 6. Tensile properties of BOL CCMs were previously measured and indicated ductile behavior under a wide range of environmental conditions.[14] After 4,000 cycles of AMST operation, the partially degraded CCMs still exhibited excellent ductile behavior similar to that of the BOL CCMs, reaching full elongation to the DMA maximum travel length without fracture. However, from 4,000 to 20,000 cycles, elongation and toughness (defined by the area below the stress-strain curve) diminished continuously and the CCM behavior gradually transformed from ductile to brittle identically in AMST-1 and AMST-2. Furthermore, the maximum tolerated stress at fracture was gradually reduced during the AMST operation. The decay in stress tolerance accompanied by the rapid drop in elongation and toughness indicates the ongoing formation and propagation of micro-cracks from BOL to 20,000 cycles due to the fatigue process. The decay in mechanical strength and ductility was relatively smooth when compared to the dramatic decay reported for the COCV AST.[43] In the case of COCV AST, the rapid decay in mechanical strength was attributed to the highly aggressive underlying chemical degradation that disintegrated the ionomer molecular structure.[43] Analogously, deterioration in mechanical properties (primarily elongation) was also observed under purely chemical degradation at constant RH.[33] In summary, it is shown here that purely mechanical membrane degradation can independently reduce the mechanical strength of the CCM and ultimately generate membrane failure; however, chemical degradation can exacerbate the decay in mechanical strength and lead to rapid failure when subjected to mechanical stress.

The detailed mechanical properties (final strain, UTS, elastic modulus) of the AMST degraded CCMs obtained from tensile testing are displayed and compared in Figure 7 as a function of the number of AMST cycles. The total elongation (elastic and plastic) of the CCM is depicted in Figure 7a. As the BOL CCMs never reached the fracture point within the DMA travel length (330% elongation), the final strain was selected to represent CCM elongation instead of fracture strain. The final strain was reduced significantly from ~300% at 4,000 cycles to 20–55% at 20,000 cycles in both AMST experiments. The rate of decay in elongation was relatively high up to 12,000 cycles and

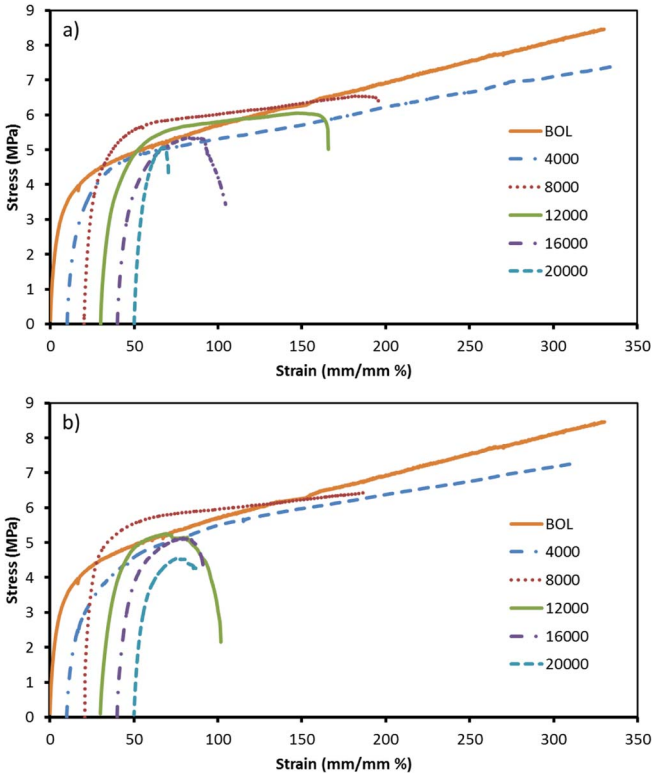

Figure 6. Tensile stress-strain curves measured at 70°C and 90% RH for partially degraded CCM samples extracted at different numbers of fatigue cycles (as indicated on the legend) during the (a) AMST-1 and (b) AMST-2 experiments. For graphical clarity, the origins were shifted by 10% strain to the right along the strain axis for each curve.

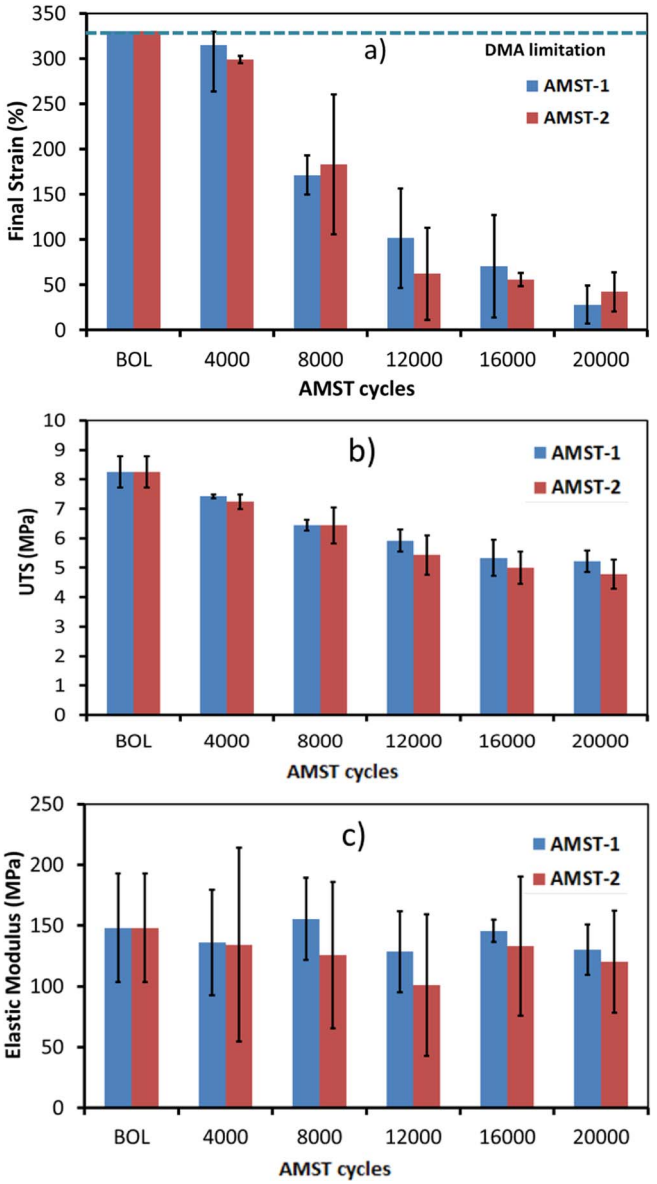

Figure 7. Evolution of CCM mechanical properties as a function of the number of AMST cycles: a) final strain; b) ultimate tensile strength (UTS); and c) elastic modulus.

then slowed down until 20,000 cycles, suggesting that the initiation of micro-cracks inside the membrane in the early stages of the AMST had stronger influence on the ductility than the propagation of cracks in the later, more mature stages of degradation. In comparison, the EOL COCV AST[43] resembled much lower final strain than the end-of-test AMST indicating a more advanced state of degradation obtained by the combined chemical and mechanical degradation mechanism. In addition, the relatively high variability in the final strain at each level of degradation indicates the highly localized nature of the mechanical degradation mechanism which is in agreement with the microstructural images represented in Figures 4 and 5. The high variability in the properties of the mechanically degraded CCMs is in contrast to the COCV AST degraded CCMs where more homogeneous decay in mechanical properties and microstructure was obtained due to chemical degradation.[31,43]

The ultimate tensile strength (UTS) of the CCM as a function of AMST cycles is depicted in Figure 7b. It was found that UTS decreased gradually from BOL to 20,000 cycles with a decelerating decay rate where the changes were less pronounced beyond 12,000 cycles. Formation of micro-cracks in the early cycles produces preferred fracture nucleation sites. However, additional crack initiation sites formed at the later stages of the experiment would not be detected in the UTS trend due to the presence of more severe, pre-existing micro-cracks that are responsible for tensile fracture of the specimen. Although the present UTS decay trend is qualitatively similar to that of the previous reported COCV AST experiment, the mechanisms are entirely different, considering that the UTS decay during COCV AST was attributed to molecular changes caused by chemical degradation.[31,43]

The elastic modulus of the CCM, representing the resistance to elastic deformation under applied stress, was calculated from the initial slope of the stress-strain curve and exhibited in Figure 7c as a function of the number of AMST cycles. No remarkable changes were observed in the elastic modulus during mechanical degradation, although high variability was present in the data. The nearly constant elastic modulus indicates that the deterioration in the ionomer molecular structure was insignificant during the fatigue process although localized changes may have occurred due to the presence of fatigue induced micro-cracks of various sizes.

Expansion properties.— The aforementioned results of tensile experiments provide useful insight into the ex-situ mechanical properties of the CCM and the state of degradation. However, under in-situ conditions, the MEA is continuously subjected to dynamic hygrothermal oscillations inducing essentially different types of stress in the CCM. A tensile test by its nature is incapable of capturing the time-dependent mechanical properties of the viscoelastic-viscoplastic PFSA ionomer membrane. The time-dependent response of the membrane to hygrothermal changes was significantly altered when subjected to isolated chemical[22] and combined chemical and mechanical degradation.[43] Hence, hygral and thermal expansion experiments were

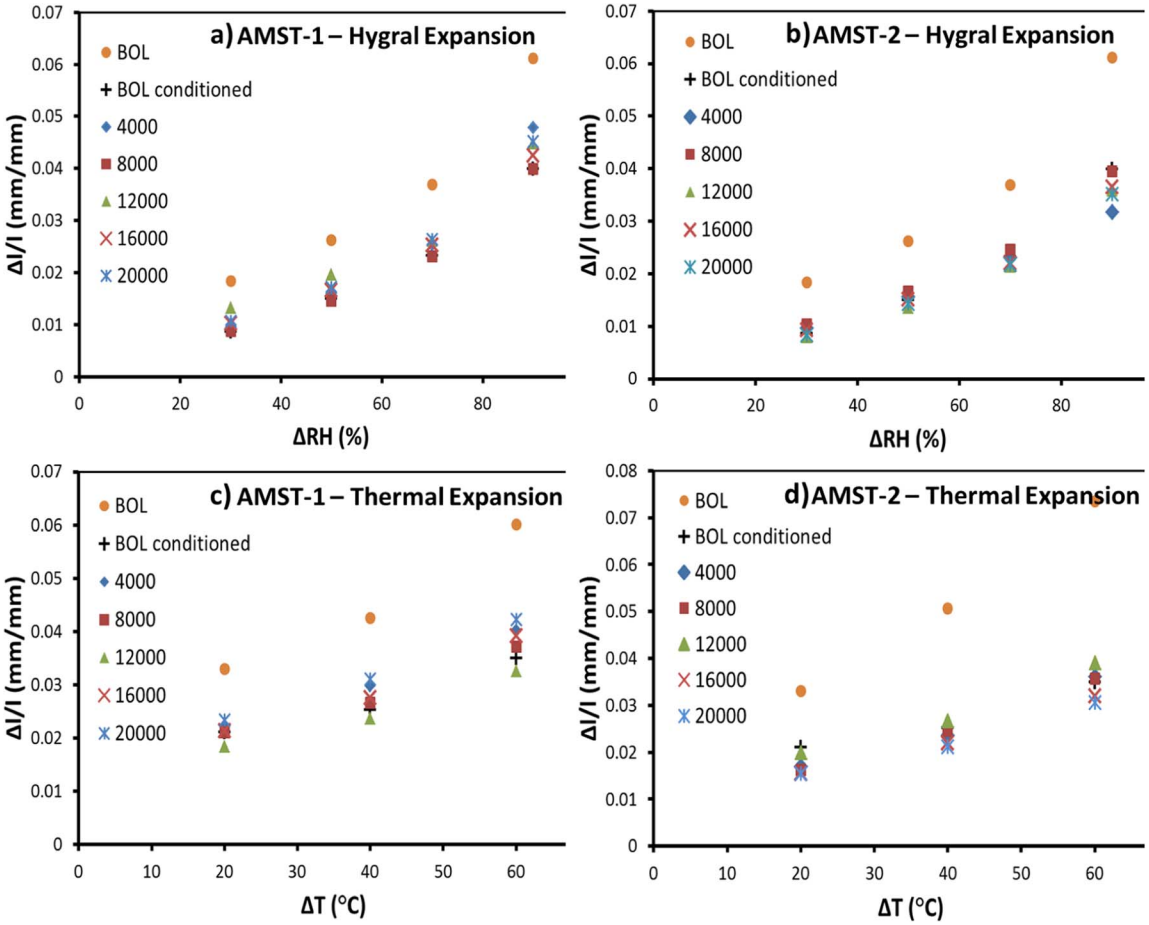

Figure 8. CCM (a.b) hygral expansion at 70°C and (c.d) thermal expansion at 90% RH measured every 4,000 cycles during (a,c) AMST-1 and (b,d) AMST-2. Thermal expansion is shown for heating from 20°C to 40°C, 60°C, and 80°C.

utilized in order to evaluate the mechanical response of the degraded CCMs to the in-situ hygrothermal swings. Figure 8 exhibits the obtained time-dependent hygrothermal responses of the CCM to the stepwise rise in RH and temperature. Each data point in Figures 8a,8b resembles the average hygral elongation of the CCM at the desired RH with respect to the initial state at 0% RH in AMST-1 and AMST-2, respectively, while the temperature was fixed at 70°C. As anticipated, the in-plane expansion due to the membrane water uptake increased gradually with RH. It is noteworthy that the hygral expansion property of the CCM was substantially reduced during the MEA conditioning process, after which the hygral expansion dropped to 65% of the BOL value at 90% RH. In contrast, from the conditioned state through to the end-of-test after 20,000 AMST cycles, the hygral expansion property remained unchanged independent of the degradation level. This finding is in stark contrast to the significant decay in hygral expansion during combined chemical and mechanical degradation[43] which was mainly attributed to chemically induced changes in the ionomer.

Figures 8c,8d exhibits the average thermal expansion of the CCM from 20°C to the desired temperature at constant 90% RH in AMST-1 and AMST-2, respectively. The gradual expansion during the temperature rise was likely due to the increase in membrane water uptake capacity and molecular thermal expansion. In agreement with the hygral expansion results, the thermal expansion of the CCM was mainly affected by conditioning, due to which the thermal expansion property was reduced to 58% of the BOL value at 80°C. No remarkable changes in thermal expansion were observed during the hygrothermal fatigue degradation, which is again consistent with the hygral expansion results. The relatively fixed expansion properties during the mechanical degradation can be correlated to the obtained elastic modulus from the tensile tests. Although expansion experiments may induce both elastic and plastic strains, the hygrothermal expansion and elastic modulus resemble the ionomer molecular resistance and bundle strength against the dimensional changes. It is in agreement with the COCV AST results[43] which led to reduction in hygrothermal expansion coefficients and increase in elastic modulus with respect to the COCV AST cycles, both indicating the elevation in membrane stiffness and resistance to elongation.

Conclusions

The evolution of microstructure and mechanical properties of catalyst coated PFSA membranes subjected to isolated mechanical fatigue degradation was investigated. Elevated hygrothermal stresses were applied to the membrane electrode assembly following two custom-developed accelerated mechanical stress test (AMST) procedures to create partially fatigue degraded CCMs for further mechanical and microstructural analyses. Cross sectional and top surface SEM images of the end-of-test CCMs revealed formation of mechanically induced damage including membrane and catalyst layer cracks as well as delamination as a result of cyclic tensile and compressive fatigue stress. The damage generated by the second AMST experiment was shown to be more severe than the first experiment due to the higher temperature and larger fatigue stress amplitude although the overall MEA leak rates were on the same order of magnitude, close to the membrane failure criterion. Tensile testing demonstrated that membrane fatigue can reduce the mechanical strength of the CCM in the absence of chemical stressors. In this manner, ultimate tensile strength, final strain, and fracture toughness were reduced significantly with similar trends in both experiments indicating the transformation in material behavior from ductile to relatively brittle due to the initiation

and propagation of micro-cracks. In contrast, the elastic modulus and hygral and thermal expansion properties were relatively constant during the fatigue process, except for a moderate reduction in expansion during MEA conditioning. This indicates that the mechanical fatigue does not alter the elastic behavior of the CCM and its response to hygrothermal fluctuations during dynamic fuel cell operation. Overall, the observed decay in mechanical strength and its linkage to the microstructural damage reveals the crucial role of mechanical fatigue degradation in the initiation and propagation of membrane failures. Development of mitigation strategies to limit the in-situ mechanical stresses is therefore essential for accomplishing the fuel cell durability and lifetime goals. Further analysis on the nature of crack initiation and subsequent crack propagation would also be useful in order to enhance the fundamental understanding of the mechanical membrane degradation phenomena.

Acknowledgments

Automotive Partnership Canada (APC), Ballard Power Systems, and the Natural Sciences and Engineering Research Council (NSERC) are gratefully acknowledged for funding this project. Ballard Power Systems are also acknowledged for providing access to experimental facilities and technical support. The authors thank Marc-Antoni Goulet, Ileana Co, Wendy Tian, Anudeep Chohan, Ossama Mansoor, Ali Bhangu, and Will Kim for experimental assistance.

References

1. Y. Yu, H. Li, H. Wang, X. Z. Yuan, G. Wang, and M. Pan, *J Power Sources*, **205**, 10 (2012).
2. J. Wu, X. Z. Yuan, J. J. Martin, H. Wang, J. Zhang, J. Shen, S. Wu, and W. Merida, *J Power Sources*, **184**, 104 (2008).
3. F. D. Coms, *ECS Trans*, **16**, 235 (2008).
4. S. Zhang, X. Yuan, H. Wang, W. Merida, H. Zhu, J. Shen, S. Wu, and J. Zhang, *Int J Hydrogen Energy*, **34**, 388 (2009).
5. K. H. Wong and E. Kjeang, *Chem Sus Chem*, **8**, 1072 (2015).
6. L. Ghassemzadeh and S. Holdcroft, *J AM CHEM SOC*, **135**, 8181 (2013).
7. J. T. Hinatsu, M. Mizuhata, and H. Takenaka, *J Electrochem Soc*, **141**, 1493 (1994).
8. S. Kundu, L. C. Simon, M. Fowler, and S. Grot, *Polymer*, **46**, 11707 (2005).
9. Y. Tang, A. M. Karlsson, M. H. Santare, M. Gilbert, S. Cleghorn, and W. B. Johnson, *Mat Sci Eng A*, **425**, 297 (2006).
10. F. Bauer, S. Denneler, and M. Willert-Porada, *J Polym Sci Pol Phys*, **43**, 786 (2005).
11. H. Tang, S. Peikang, S. P. Jiang, F. Wang, and M. Pan, *J Power Sources*, **170**, 85 (2007).
12. R. M. H. Khorasany, A. Sadeghi Alavijeh, E. Kjeang, G. G. Wang, and R. K. N. D. Rajapakse, *J Power Sources*, **274**, 1208 (2015).
13. X. Huang, R. Solasi, Y. Zou, M. Feshler, K. Reifsnider, D. Condit, S. Burlatsky, and T. Madden, *J Polym Sci Pol Phys*, **44**, 2346 (2006).
14. M. A. Goulet, R. M. H. Khorasany, C. De Torres, M. Lauritzen, E. Kjeang, G. G. Wang, and N. Rajapakse, *J Power Sources*, **234**, 38 (2013).
15. R. M. H. Khorasany, M. A. Goulet, A. Sadeghi Alavijeh, E. Kjeang, G. G. Wang, and R. K. N. D. Rajapakse, *J Power Sources*, **252**, 176 (2014).
16. A. Sadeghi Alavijeh, R. M. H. Khorasany, A. Habisch, G. G. Wang, and E. Kjeang, *J Power Sources*, **285**, 16 (2015).
17. M. A. Goulet, S. Arbour, M. Lauritzen, and E. Kjeang, *J Power Sources*, **274**, 94 (2015).
18. M. P. Rodgers, L. J. Bonville, H. Russell Kunz, D. K. Slattery, and J. M. Fenton, *Am Chem Soc*, **112**, 6075 (2012).
19. S. Zhang, X. Z. Yuan, J. N. C. Hin, H. Wang, J. Wu, K. A. Friedrich, and M. Schulze, *J Power Sources*, **195**, 1142 (2010).
20. J. Wu, X. Z. Yuan, J. J. Martin, H. Wang, D. Yang, J. Qiao, and J. Ma, *J Power Sources*, **195**, 1171 (2010).
21. H. Zhang and P. K. Shen, *Chem Rev*, **112**, 2780 (2012).
22. Y. P. Patil, W. L. Jarrett, and K. A. Mauritz, *J Membrane Sci*, **356**, 7 (2010).
23. M. Zhao, W. Shi, B. Wu, W. Liu, J. Liu, D. Xing, Y. Yao, Z. Hou, P. Ming, and Z. Zou, *Electrochim Acta*, **153**, 254 (2015).
24. Y. H. Lai, C. K. Mittelsteadt, C. S. Gittleman, and D. A. Dillard, *J Fuel Cell Sci Tech*, **6**, 021002 (2009).
25. J. Kang and J. Kim, *Int J Hydrogen Energ*, **35**, 13125 (2010).
26. R. Banan, A. Bazylak, and J. Zu, *Int J Hydrogen Energ*, **40**, 1911 (2015).
27. G. De Moor, C. Bas, F. Lesage, A. S. Dane, E. Claude, E. Rossinot, M. Paris, L. Flandin, and N. D. Alberola, *J Appl Polym Sci*, **120**, 3501 (2011).
28. T. T. Aindow and J. O'Neill, *J Power Sources*, **196**, 3851 (2011).
29. S. Vengatesan, M. W. Fowler, X. Z. Yuan, and H. Wang, *J Power Sources*, **196**, 5045 (2011).
30. N. S. Khattra, A. M. Karlsson, M. H. Santare, P. Walsh, and F. C. Busby, *J Power Sources*, **214**, 365 (2012).
31. C. Lim, L. Ghassemzadeh, F. Van Hove, M. Lauritzen, J. Kolodziej, G. G. Wang, S. Holdcroft, and E. Kjeang, *J Power Sources*, **257**, 102 (2014).
32. C. Lim, A. Sadeghi Alavijeh, M. Lauritzen, J. Kolodziej, S. Knights, and E. Kjeang, *ECS Electrochem Lett*, **4**, F29 (2015).
33. N. Macauley, A. Sadeghi Alavijeh, M. Watson, J. Kolodziej, M. Lauritzen, S. Knights, G. Wang, and E. Kjeang, *J Electrochem Soc*, **162**, F98 (2015).
34. N. Macauley, L. Ghassemzadeh, C. Lim, M. Watson, J. Kolodziej, M. Lauritzen, S. Holdcroft, and E. Kjeang, *ECS Electrochem*, **2**, F33 (2013).
35. M. Aoki, H. Uchida, and M. Watanabe, *Electrochem Commun*, **8**, 1509 (2006).
36. N. Macauley, K. H. Wong, M. Watson, and E. Kjeang, *J Power Sources*, **299**, 139 (2015).
37. W. Gu, R. N. Carter, P. T. Yu, and H. A. Gasteiger, *ECS Trans*, **11**, 963 (2007).
38. D. Zhao, B. L. Yi, H. M. Zhang, and M. Liu, *J Power Sources*, **195**, 4606 (2010).
39. M. P. Rodgers, L. J. Bonville, and D. K. Slattery, *ECS Trans*, **41**, 1461 (2011).
40. N. E. Cipollini, *ECS Trans*, **11**, 1071 (2007).
41. S. Helmly, R. Hiesgen, T. Morawietz, X. Z. Yuan, H. Wang, and K. A. Friedrich, *J Electrochem Soc*, **160**, F687 (2013).
42. M. P. Rodgers, B. P. Pearman, L. J. Bonville, D. A. Cullen, N. Mohajeri, and D. K. Slattery, *J Electrochem Soc*, **160**, F1123 (2013).
43. A. Sadeghi Alavijeh, M. A. Goulet, R. M. H. Khorasany, J. Ghataurah, C. Lim, M. Lauritzen, E. Kjeang, G G. . Wang, and R. K. N. D. Rajapakse, *Fuel Cells*, **15**, 204 (2015).
44. U.S. Department of Energy, DOE CELL COMPONENT ACCELERATED STRESS TEST, (2010) http://www1.eere.energy.gov/hydrogenandfuelcells/pdfs/component_durability_may_2010.pdf.
45. Y. Li, D. A. Dillard, Y. H. Lai, S. W. Case, M. W. Ellis, M. K. Budinski, and C. S. Gittleman, *J Electrochem Soc*, **159**, B173 (2012).
46. R. M. H. Khorasany, E. Kjeang, G. G. Wang, and R. K. N. D. Rajapakse, *J Power Sources*, **279**, 55 (2015).